Magnetic Flux-Trapping of Anisotropic-Grown Y-Ba-Cu-O Bulk Superconductors during and after Pulsed-Field Magnetizing Processes

T Oka[1], Y Yamada[1], T Horiuchi[1], J Ogawa[1], S Fukui[1], T Sato[1], K Yokoyama[2], M Langer[3]

[1] Niigata University, 8050 Ikarashi-2-nocho, Nishi-ward, Niigata 950-2181, Japan

[2]Ashikaga Institute of Technology, 268-1 Ohmae-cho, Ashikaga, Tochigi 326-8558 Japan

[3]IFW Dresden, Helmholzstr. 20-01069 Dresden, Germany

E-mail: okat@eng.niigata-u.ac.jp

Abstract. The magnetic flux penetration into the melt-textured Y-Ba-Cu-O high temperature superconducting bulk magnets were precisely evaluated during and after the pulsed field magnetization processes operated at 30 K. The bulk magnets were carefully fabricated by the cold seeding method with use of a single and a pair of seed crystals composed of the Nd-Ba-Cu-O thin films. These seed crystals were put on the top surfaces of the precursors to let the large grains grow during the heat treatments. We observed the flux penetrations which occurred in the lower applied-field regions at around 3.1 T for the samples bearing the twin seeds than those of the single-seeded crystals at around 3.8 T. This means that the magnetic fluxes are capable of invading into the twin-seeded samples more easily than the single-seeds. It suggests that the anisotropic grain growths of parallel and normal to the rows of seed crystals affects the variations of J_c values with different distributions of the pinning centers, results in the preferential paths for the invading magnetic fluxes.

1. Introduction

The high temperature superconducting (hereafter abbreviated as HTS) materials fabricated by so-called melt-processes have a unique characteristic to act as the trapped-field magnets or bulk magnets [1-3]. Some investigations including our previous studies have been performed on the pulsed-field magnetization (PFM) methods to develop more compact and easier processes than the field cooling (FC) method [4, 5]. The fact that the field-trapping performance on the PFM process is usually inferior to those by the FC method is attributed to the local heating which is mainly caused by the motion of the applied magnetic flux in the superconducting phases in the sample [6, 7].

The keys for high field-trapping are the temperature controlling [8] and the consecutive magnetic pulsed-field application in the magnetizing processes [9]. Fujishiro *et al.* reported the highest performance of 5.2 T with the precise analysis on the trapped-field distributions throughout the activation processes [10, 11]. The trapped-field distributions which remain in the bulk magnet before the following activation affect the magnetic flux motion in the sample and resultant field-trapping [12].Therefore, it is definitely important to clarify the behaviors of the invading flux into the bulk magnets during the PFM processes in order to enhance their field-trapping ability.

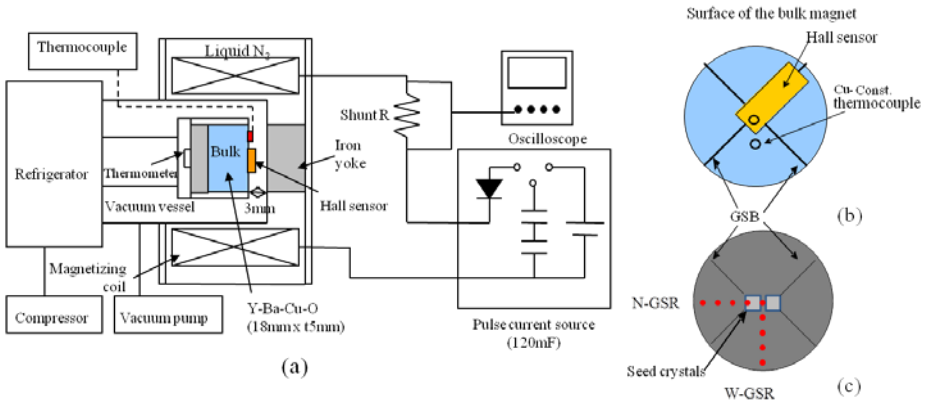

Fig. 1. Schematic illustration of the bulk magnet system (a), the positions of sensors on the sample surface (b), and the positions of EPMA analysis as a function of distance from the centre along the narrow-GSR and wide-GSR directions (c).

The melt-processed bulk magnets show the heterogeneous microstructures according to the presence of non-superconducting Y_2BaCuO_5 (Y211) particles which must contribute to enhance the J_c values [13]. In this paper, the bulk magnets bearing the anisotropic structure were fabricated so as to examine how the field-penetration occurs when the intense magnetic pulsed-fields are applied to the samples in their superconducting states. We attempt to examine the flux motions by discussions on the data of the trapped-flux densities.

2. Experimental

2.1 Sample preparation and structural analysis

The starting powers of $YBa_2Cu_3O_{7-\delta}$ (Y123) and Y211were mixed in the proper ratios with 1 wt% CeO_2 addition and pressed into the pellets. The Y211 nominal content was chosen as 28.5% in molar ratio. The precursors were heat-treated in the cold seeding method with the Nd-Ba-Cu-O thin films on the MgO crystal substrates (THEVA Co.), and heated to 1050 ^oC and then gradually solidified with the cooling rate 0.25 ^oC/h. The post annealing was operated in the temperature range of 500 – 300 ^oC for 167 hours in the flowing pure oxygen atmosphere. The compositional analysis was operated with use of the electron probe micro analyzer EPMA (JEOL Ltd, JXA-8621MX).

2.2 Pulsed-field magnetization procedure

An illustrated structure of the total system is shown in Fig. 1(a) with the electrical circuit which is equipped with a condenser bank of 120 mF (Nihon Denji Sokki Co., SBV-10124), a shunt resister, and an oscilloscope. Figure 1(c) shows the points of EPMA compositional analyses, which were operated along the directions parallel and normal to the row of seed crystals. We defined the direction along the row of seed crystals as narrow side of the growth sector region (abbreviated as n-GSR) and as wide side (w-GSR) which is normal to it.

Sample	#1	#2	#3	#4	#5
Seed crystal	-	Gap 2.5mm	twin	twin	twin
Growth period	80h	80h	80h	80h	60h

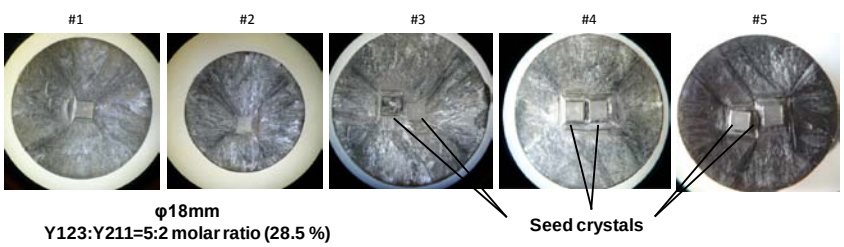

Fig. 2. Anisotropic-Grown Y-Ba-Cu-O Bulk Superconductors with various seed-crystal positions.

3. Results and discussions

3.1 Anisotropic-grown HTS bulk magnets

Figure 2 shows the topside-views of the bulk magnet samples, which were fabricated by the melt-process with varying the positions and numbers of seed crystals. The sample size is approximately 15 mm in diameter. One sees the apparent growth sector boundaries (GSB), which indicate their characteristic "X-shape". We note that #1 sample is the conventional single-seeded sample, #2 is the sample bearing the single-seed whose position was displaced 2.5 mm distance from the center, and #3 – 5 are twin-seeded crystals which exhibited the anisotropic crystal growth. The GSB lines for #3 – 5 samples divide the anisotropic-grown GSR in the narrow and the wide portions along the direction parallel to the rows of seed crystals and normal to them, respectively. Since the GSB lines starts at the corner of the seed crystals, the neighboring corners draw no GSB lines. Therefore, we see the narrow GSRs along the direction parallel to the row of seed crystals and the wide GSRs along the direction normal to it, as shown in Fig. 1(c).

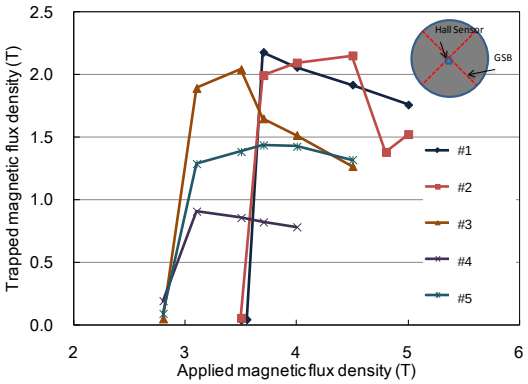

Fig. 3. Experimental results of trapped flux of HTS bulk samples with various seeding patterns after PFM.

3.2 Trapped-fields in the bulk magnets after and during PFM process

The trapped magnetic flux densities which were measured at the center of each pulsed-field application are shown in Fig. 3. One sees that the starting points of the field invasions varied with each samples. We notice that the profiles can be separated in two groups. The magnetic flux did not invade into the center of the sample until when the applied field exceeded over 3.5 T in the single-seeded crystal (#1 and 2), whereas the samples #3 – 5 easily allowed the flux invasion even when the applied field of 3 T was applied. This implies that the anisotropic grain growth structure led by the twin seeds must result in the different flux invasion behaviors into the samples. We should pay attention to the fact that the highest trapped-field of #3 and #1 are comparable and showing a similar degradation behavior caused by the heat generation after showing each peak.

Figure 4 shows the evolutional profiles of magnetic flux invasion in sample #6 twin-seeded crystal as a function of applied field. Although the speeds of the invading fluxes were similar in any magnitudes of fields, the moments when the fields started to invade moved forward with increasing applied fields. Figure 5 shows the times for the fluxes to arrive at 0.5 T from the beginnings of invasion. The profiles of arriving times are roughly separated into two groups, and the magnetic flux invades earlier and in the weaker field ranges in the twin-seeded crystals than single-seeded. This means that the introduction of the flux was promoted in the anisotropic-grown samples.

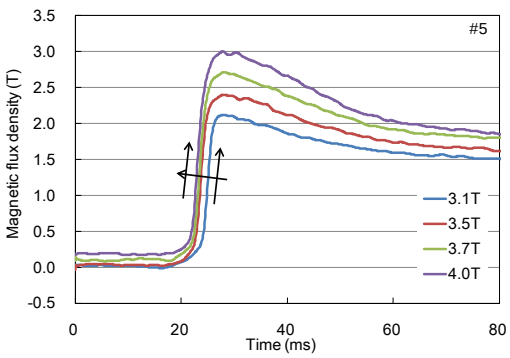

Fig. 4. Time evolutional profiles of magnetic flux invasion as a function of applied field strength.

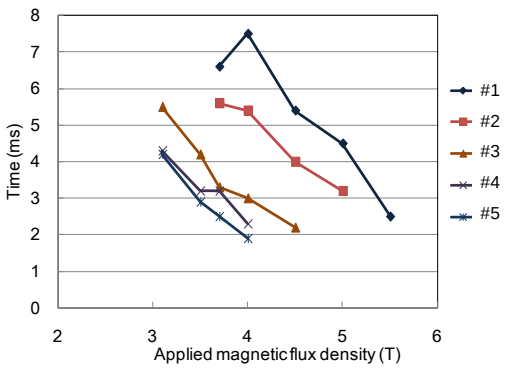

Fig.5. Arriving times of the invading flux at 0.5 T at the center point of the sample.

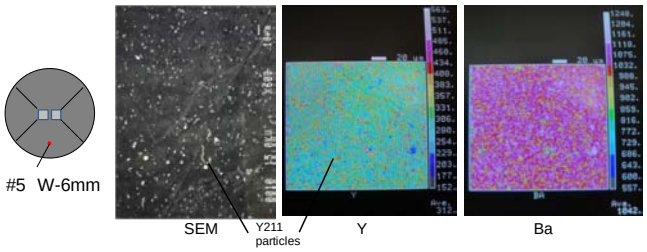

Fig.6. SEM imaging and EMPA mapping of Y and Ba detected at 6 mm distant from the center along w-GSR direction.

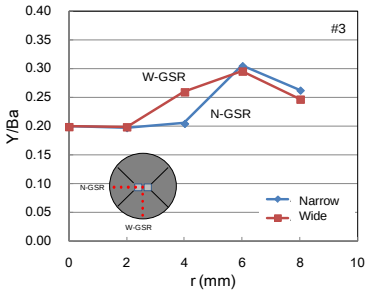

Fig. 7. Distribution of the detected characteristic X-ray intensity ratios Y/Ba along the n- and w-GSR directions.

3.3 Compositional analysis

We operated the compositional analysis on the sample with use of EPMA. Figure 6 shows the SEM image and mapping of compositions Y and Ba at the point 6 mm distant from the center along the w-GSR. One sees the uniformly dispersed Y211 particles and the mapping approves it. It is known that the Y211 particles do not precipitate under the regions where the seed crystals are placed due to the pushing effect at the boundaries of melt and solid phases. The characteristic X-ray signals should exhibit the varieties of their distributions. Figure 7 shows the intensity ratios of Y and Ba measured at various points along the directions n-GSR and w-GSR. We observed a distinct difference in Y/Ba at the position 4 mm distant from the centre point. This implies the anisotropic distributions of Y211, and suggests the different J_c distribution between the directions along n- and w-GSRs.

4. CONCLUSION

The field-trapping behaviors of the anisotropic-grown Y-Ba-Cu-O-based bulk magnets with use of single, displaced, and twin-seeded crystals were evaluated with respect for the trapped-flux density during and after PFM processes. The magnetic flux invades the twin-seeded sample earlier and easier than single-seeded crystals. The inhomogeneous distribution of Y211, which is introduced in the material structure by controlling the crystal growth, affects the flux invasion behaviors. The results suggest the easier, calmer activation method for the HTS bulk magnets than usual PFM process.

References

[1] Weinstein R, Chen In-Gann, Liu J and K Lau 1991 *J. Appl. Phys.* **70** 6501
[2] Krabbes G, Fuchs G, Schatzle P, Gruss S, Park J, Hardinghaus F 2000 *Advances in Superconductivity XII Tokyo Springer-Verlag* 437
[3] Tomita M and Murakami M 2003 *Nature* **421** 517
[4] Oka T, Itoh Y, Yanagi Y, Yoshikawa M, Ikuta H Mizutani U 2000 *Physica C* **335** 101
[5] Ikuta H, Ishihara H. Yanagi Y, Itoh Y, Mizutani U 2002, *Supercond. Sci. Technol*. **15,** 606
[6] Itoh Y, Mizutani U 1996 *Jpn J Appl Phys*, **35,** 2114
[7] Mizutani U, Mase A, Tazoe K, Ikuta H, Oka T, Itoh Y, Yanagi Y, Yoshikawa M 2000 *Physica C* **335** 92
[8] Sander M, Sutter U, Koch R, Klaeser M 2000 *Supercond. Sci. Technol.* **13** 841
[9] Mizutani U, Oka T, Itoh Y, Yanagi Y, Yoshikawa M, Ikuta H 1998 *Applied Superconductivity* **6** 235
[10] Fujishiro H, Tateiwa T, Fujiwara A, Oka T, Hayashi H 2006 *Physica C* **445-448** 334
[11] Fujishiro H, Hiyama T, Tateiwa T, Yanagi Y, Oka T 2007 *Physica C* **463-465** 394
[12] Oka T, Seki H, Ishiduka D, Ogawa J, Fukui S, Sato T, Yokoyama K, Murakami A 2012 *J. Phys. Conf. Ser.* **400** 022089
[13] Oka T, Itoh Y, Yanagi Y, Tanaka H, Takashima S, Yamada Y, Mizutani U 1992 *Physica C* **200** 55